Taylor & Francis
Taylor & Francis Group

Journal of Maps

ISSN: (Print) (Online) Journal homepage: https://www.tandfonline.com/loi/tjom20

Map of tectonic shortening structures in Chryse Planitia and Arabia Terra, Mars

Savana Z. Woodley, Peter Fawdon, Matthew R. Balme & David A. Rothery

To cite this article: Savana Z. Woodley, Peter Fawdon, Matthew R. Balme & David A. Rothery (2023) Map of tectonic shortening structures in Chryse Planitia and Arabia Terra, Mars, Journal of Maps, 19:1, 2251514, DOI: 10.1080/17445647.2023.2251514

To link to this article: https://doi.org/10.1080/17445647.2023.2251514

JOURNAL OF MAPS
2023, VOL. 19, NO. 1, 2251514
https://doi.org/10.1080/17445647.2023.2251514

Map of tectonic shortening structures in Chryse Planitia and Arabia Terra, Mars

Savana Z. Woodley, Peter Fawdon, Matthew R. Balme and David A. Rothery

School of Physical Sciences, The Open University, Milton Keynes, UK

ABSTRACT

We present a 1:4,000,000 scale map of tectonic landforms in Chryse Planitia and Arabia Terra, on either side of Mars' dichotomy. Our study area is a ~3 million km^2 region, transitional between Mars' highlands and lowlands including Oxia Planum, the landing site of the ExoMars rover. Using a structural mapping approach, we digitised all kilometre-scale tectonic structures at a scale of 1:50,000 using high-resolution data (~6 m/pixel). Although this region is represented as sparsely tectonised on global tectonic maps, we find evidence of widespread tectonic shortening structures across the region. The shortening structures have a dominant N-S orientation and occur in all globally identified geological units. The structural map contributes to a broader understanding of the geological history of the region and Mars' wider tectonic history.

ARTICLE HISTORY
Received 29 May 2023
Revised 6 August 2023
Accepted 17 August 2023

KEYWORDS
Mars; planetary tectonism; shortening structures; wrinkle ridges; lobate scarps; ExoMars

Key Policy Highlights

- We present a structural map of tectonic thrust-fault related landforms, termed shortening structures, in Chryse Planitia and Arabia Terra, Mars.
- Using CTX, THEMIS, MOLA, and HRSC data, we identify and digitise 845 shortening structures.
- Shortening structures have a dominant N-S orientation and occur in geological units of all ages.

1. Introduction

Tectonic landforms on Mars have previously been globally mapped using 100–300 m/pixel Viking images (Wellman et al., 1976), 1 km/pixel MOLA hillshades (Mars Observer Laser Altimeter; Smith et al., 2001), and 100 m/pixel THEMIS images (Thermal Emission Imaging System; Christensen et al., 2004) and MOLA topography at 1:20,000,000 (Watters, 1993; Anderson et al., 2001, 2008; Knapmeyer et al., 2006; Tanaka et al., 2014; Figure 1A). Since these studies were completed, a near-global coverage of high-resolution ~6 m/pixel CTX images (Context Camera; Dickson et al., 2023; Malin et al., 2007) has developed. This provides the opportunity to map and study tectonic landforms in far greater detail than previously possible.

The tectonic landforms along the dichotomy between the Chryse Planitia lowlands and the Arabia Terra highlands (Figure 1B) have not previously been mapped or quantitively studied using high resolution data. The region comprises predominantly Noachian (~4.1–3.7 Gyr) and Hesperian (~3.7–3.0 Gyr) terrain (Hartmann & Neukum, 2001; Quantin-Nataf et al., 2021; Tanaka et al., 2014), with a complex geological history and stratigraphy that includes the deposits of extensive river systems (Davis et al., 2016, 2023; Fawdon et al., 2022). Oxia Planum (Figure 1B), the intended landing site of the ExoMars rover, is located in this transitional region between the ancient highlands and younger lowland terrains (Vago et al., 2015). High resolution tectonic mapping can provide insights into the timing of tectonic activity in this region, and contribute to a wider understanding of Mars' global tectonic history, and of the evolution and properties of its lithosphere. Additionally, high-resolution mapping will provide tectonic context for the ExoMars rover mission.

The impact of tectonism, at both regional and global scale, on the geological history of Chryse Planitia and Arabia Terra is poorly understood. Thus, to provide constraints on the region's tectonic evolution, we present a map of tectonic landforms of a ~3 million km^2 study area that straddles Mars' global dichotomy (Figure 1; Woodley et al., 2023). Sparse tectonic landforms have previously been identified in the study area; although this region is represented as sparsely tectonised on global tectonic maps (e.g. Anderson et al., 2001, 2008; Knapmeyer et al., 2006; Tanaka et al., 2014; Watters, 1993), we identify widespread tectonic landforms termed shortening structures. Shortening structures are tectonic landforms interpreted as the surface expression of thrust-faults with various degrees of folding (including landforms previously

CONTACT Savana Z. Woodley savana.woodley@open.ac.uk School of Physical Sciences, The Open University, Milton Keynes, Buckinghamshire MK7 6AA, UK

Supplemental data for this article can be accessed online at https://doi.org/10.1080/17445647.2023.2251514.

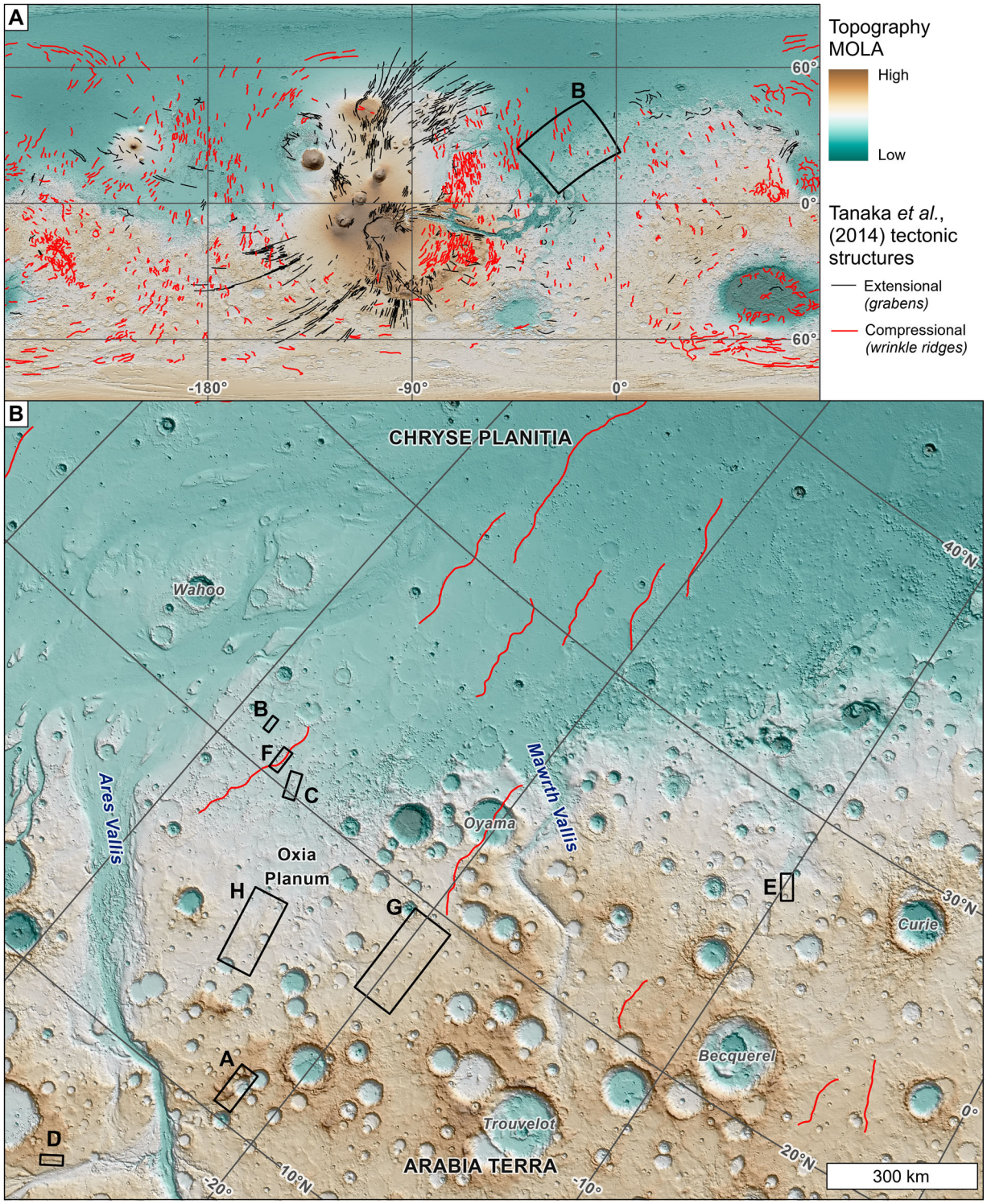

Figure 1. Location and context of the study area. **A)** Global setting of the study area (the labelled box) with linework showing previously mapped structures resulting from extensional and compressional tectonism (Tanaka et al., 2014). **B)** Extent of study area. Oxia Planum is the landing site for the ExoMars rover. Boxes show the location and extent of Figure 2 panels. Mars Orbiter Laser Altimeter (MOLA) hillshade overlain by MOLA digital elevation model.

described morphologically as wrinkle ridges or lobate scarps; e.g. Golombek & Phillips, 2010).

2. Methods

2.1. Location and projection

The map covers an area between 3–45°N and 43–358° W, forming a 1590 km x 1950km rectangle aligned obliquely to follow the dichotomy, and has an area of ~3 million km^2 (Figure 1B). The map is presented in a Hotine Oblique Mercator projection (azimuth 37°, centre latitude 23°, centre longitude −20°; Hotine, 1946) using the IAU Mars 2000 Sphere.

Elevation in the map area ranges between −6450 and 693 m relative to the MOLA datum, and there is a regional slope of <1° dipping north-westward. The southeast of the map area is located in western Arabia

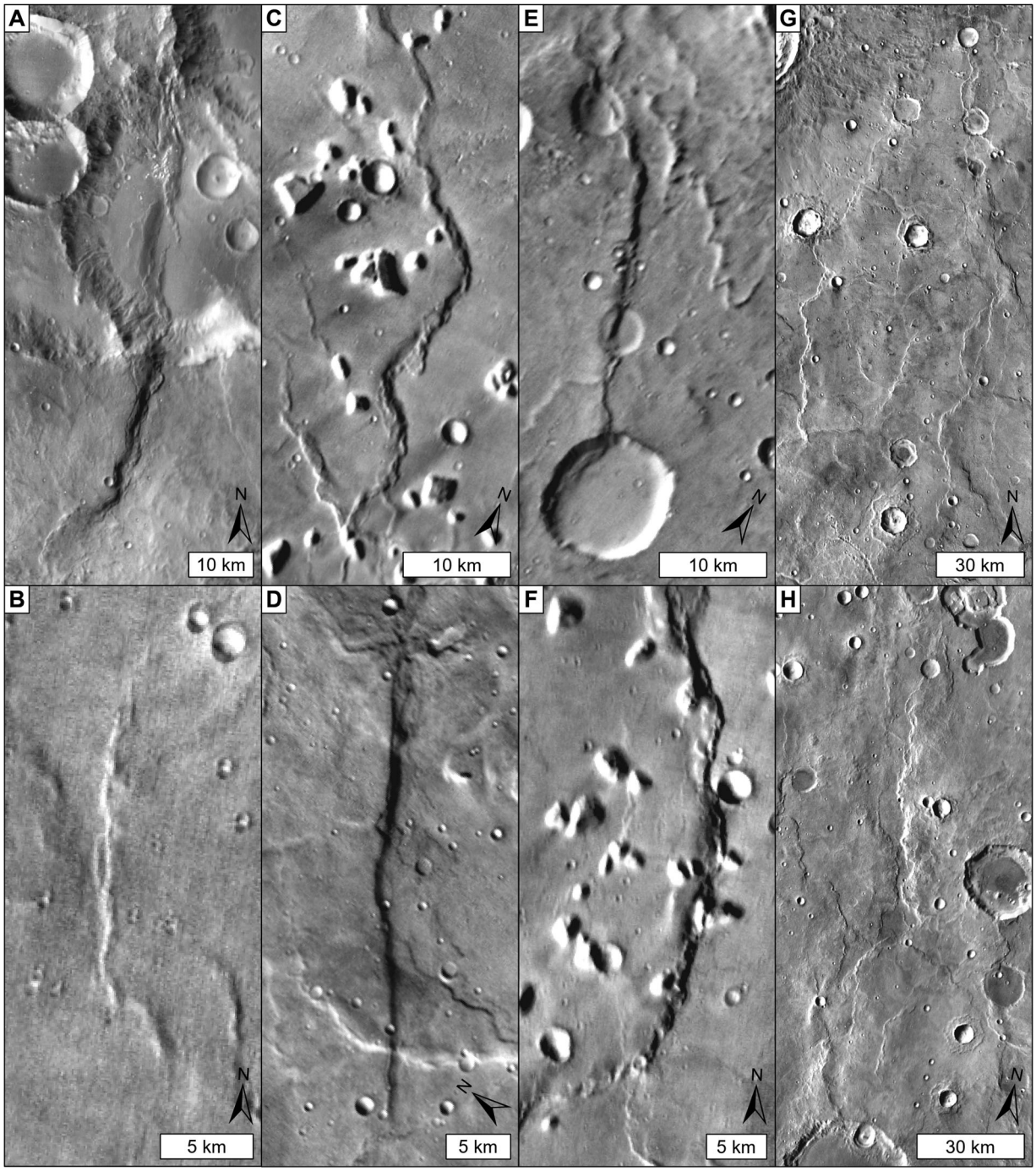

Figure 2. Example of tectonic shortening structures in the map area. THEMIS Day IR images and the location and extent of panels is shown in Figure 1B. Panels show a large variety in appearance, such as large and small structures (**A** and **B**) and sinuous and linear structures (**C** and **D**). Shortening structures deform impact craters (**A** and **E**) and mounds (**C** and **F**) and have complex planform patterns (**G** and **H**).

Terra, predominantly formed by Noachian highland units (eNh, mNh, lNh; Tanaka et al., 2014). The northwest of the map area is located in eastern Chryse Planitia, comprising Hesperian transition (Htu, eHt, Ht Hto, lHt) and lowland (lHl) units (Tanaka et al., 2014).

2.2. Data

We used Mars spacecraft remote sensing data to map kilometre-scale tectonic structures, combining visible, thermal, and topographic data products. We primarily used 793 individual ~6 m/pixel CTX images and the ~100 m/pixel THEMIS daytime infrared global mosaic (Edwards et al., 2011) to identify and digitise structures. To aid in structure identification, topographic data was viewed as a semi-transparent layer, including digital elevation models (DEMs) derived from gridded 463 m/pixel (265 pixels per degree) MOLA data and HRSC data (High Resolution Stereo Camera; Jaumann et al., 2007; Neukum et al., 2004). Sampling bias due to solar azimuth for visible data products (potentially under sampling east and west

striking structures) is minimised by identifying additional structures using slope maps and using simulated illumination (from azimuths 45° and 315°) products generated from MOLA and HRSC DEMs.

2.3. Classification

There are two types of mapping approaches for thrust-fault related landforms, a descriptive morphology-based approach (e.g. Watters, 1988, 1993) and an interpretive structural-based approach (e.g. Byrne et al., 2014). The morphology-based approach is widely used and based on qualitative descriptions, grouping structures into three categories (wrinkle ridges, lobate scarps, and high-relief ridges; e.g. Watters, 1988, 1993). However, this classification breaks down for many individual structures, which may transition morphologically as demonstrated by 'wrinkle ridge – lobate scarp transitions' (Howard & Muehlberger, 1973; Lucchitta, 1976) and 'lobate scarp – high-relief ridge transitions' (Watters & Nimmo, 2010).

As there is no clear quantitative distinction between morphological categories (Loveless et al., 2023), we opted to use an interpretive structural-based approach to map tectonic features. This is similar to mapping conducted on Mercury (Byrne et al., 2014) where thrust-fault related landforms are grouped under the term 'shortening structures' (see discussion in Byrne et al. (2018) and Klimczak et al. (2019)). We use this structural-based mapping approach, fundamentally relying on the interpretation that these landforms have a tectonic origin. We identify and interpret shortening structures as tectonic, based on: a linear-arcuate planform appearance, an asymmetric profile with a steep limb and a shallow limb (with the exception of asymmetric crenulations), and classic fault-related morphologies and attributes such as postdating crater-rim displacements, en-echelon crenulations, imbricate appearance, and push-up structures (e.g. Fossen, 2010).

We have found some extensional tectonic structures within the study area, but they are too small to be displayed at map publication scale and were therefore not digitised. These include tectonically-induced fractures tens of metres in scale (Apuzzo et al., 2021) and small grabens occurring parasitically on large shortening structures, resembling equivalent examples recently recognised to be widespread on Mercury (Man et al., in press).

2.4. Digitisation and errors

We digitised tectonic shortening structures in ArcGIS Pro 2.7.2 software as polylines at a scale of 1:50,000. If there was ambiguity in tectonic origin caused by, for example, proximity to impact ejecta, impact-sculpted terrain, or erosional scarps, the feature was excluded. We drew the polyline at the intersection between the hanging wall and the footwall, along the break in slope. Following convention, a sawtooth symbol on the polyline records fault-plane dip direction of the inferred underlying thrust fault. This direction is based on the assumption that the steepest limb forms the leading edge/forelimb of the tectonic landform and indicates the orientation of the underlying fault, although we recognise that this is not always the case (e.g. Schultz, 2000).

We calculated the geodesic *length* of each shortening structure, defined as the trace length in map view, after digitisation (length uncertainty is 2.3% based on repeat digitisation; Woodley et al., 2023). We measured the *height*, defined as the maximum scarp height of the leading edge, using the gridded MOLA DEM. We generated multiple parallel profiles where relief visually appeared largest, perpendicular to the shortening structure, and recorded the maximum elevation difference as the height (height uncertainty is 5.8% based on repeat digitisation; Woodley et al., 2023). In addition to length and height, the following properties were recorded in the attribute table (Woodley et al., 2023): scarp height class (<50 m, 50–100 m, or >100 m), morphological complexity (scarp-like, broad arch, crenulation, or broad arch and crenulations), degree of erosion (minimally eroded, eroded, heavily eroded), and orientation (linear directional mean as compass orientation).

3. Results

Widespread tectonic shortening structures occur across the map area. The distribution of the 845 shortening structures is shown in a sample map (Figure 3) and in the Map of Tectonic Shortening Structures in Chryse Planitia and Arabia Terra, Mars (Supplementary Materials; Woodley et al., 2023).

The total length of the 845 digitised shortening structures is ~28,000 km, with a mean structure length of 33.2 km (range: 4.2–201.8 km) and a mean height of 60 m (range: 8–691 m). The shortening structures show large variation in scale, morphological complexity, and degree of erosion. Shortening structures are more abundant in the eastern highland terrain and somewhat less so in the western lowland terrain (Figure 3). Greatest tectonic structure densities occur in four main regions (labelled A – D in Supplementary Materials), three of which are in the highlands (A, C, and D) and one in the lowlands (B). Densities are sparse in the region of Mawrth Vallis, in the northern corner of the study area, and in areas where there are large impact ejecta deposits (Figure 3 and Supplementary Materials). Shortening structures have a dominant N and S striking orientation (N striking structures have underlying fault planes interpreted as dipping eastward and S striking structures have

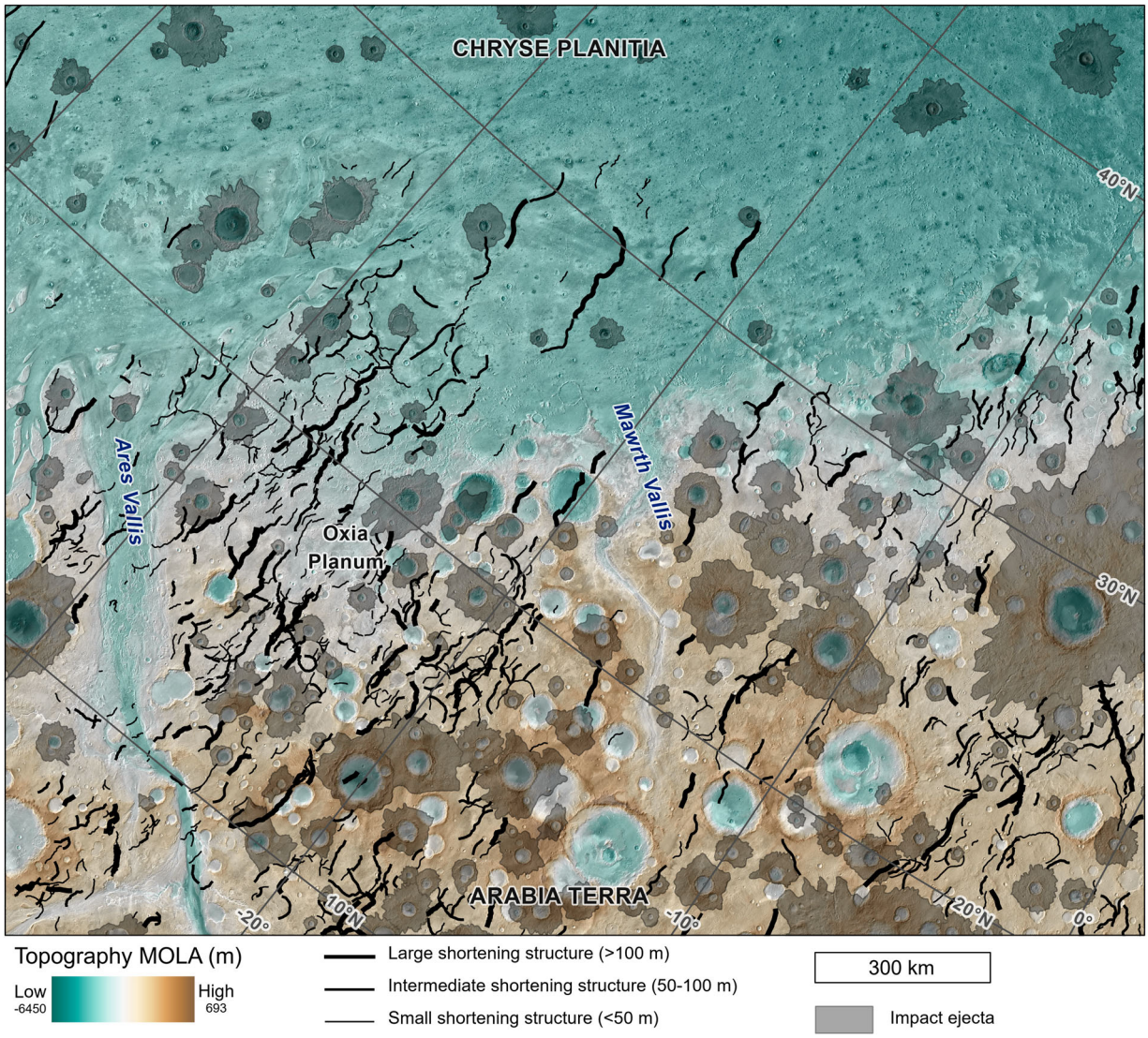

Figure 3. Sample map of tectonic shortening structures in Chryse Planitia and Arabia Terra. Symbology has been simplified – see Map of Tectonic Shortening Structures in Chryse Planitia and Arabia Terra, Mars (Supplementary Materials; Woodley et al., 2023) for full symbology. For location and extent of map, see Figure 1. THEMIS Day IR overlain by MOLA digital elevation model.

underlying fault planes interpreted as dipping westward), with only few structures striking eastward (NE to SE) or westward (SW to NW; Supplementary Materials). The E/W striking structures are dense in the same areas as the N/S striking structures (Supplementary Materials). Noticeable is the difference in length, with E/W structures being shorter (mean: 24.6 km) than N/S structures (mean: 34.5 km).

4. Discussion

4.1. Assessment of classification and digitisation method

The interpretive structural-based classification method used for digitisation in this study differs from conventional morphology-based mapping in several ways. Firstly, in the digitisation of linework; a structural-based classification does not distinguish between 'lobate scarps' and 'wrinkle ridges' and both are digitised as the break in slope at the base of the scarp rather than digitising the interpreted fold axis of wrinkle ridges (e.g. Tanaka et al., 2014). Digitising at the base of the scarp (inferred fault trace) is more consistent and objective than digitising fold axes but, at this map's publication scale, the location of fold axes compared to inferred fault traces is effectively coincident. Secondly, the terminology differs as all structures are termed *shortening structures* instead of being divided based on morphology. Although structures are grouped, their morphological complexity class is recoded in the shapefile attribute table (Woodley et al., 2023).

The morphometry data documenting shortening structures depends on the measurement methods used and thus it is important to consider these. The lengths of the shortening structures (defined as the fault trace length in map view) were calculated as geodesic lengths to prevent distortion due to map projection. However this is a simplified reflection of fault

length because: (1) A landform is often a composite of many spatially associated faults; (2) the mappable surface fault trace length is always smaller than the subsurface fault length (e.g. Kim & Sanderson, 2005); (3) small faults are not resolvable at the map scale (the shortest digitised structure is 4.2 km in length); (4) structures are mapped conservatively, which may cause underestimation of their total length, for example when structures are partly covered by impact ejecta a shorter length will be recorded. Consequently, the total mapped length represents the minimum total fault lengths.

The height of shortening structures (defined as the maximum scarp height of the leading edge) was measured by visually identifying where the height appeared largest from the MOLA DEM and slope map, and then drawing multiple MOLA topographic profiles perpendicular to the structure to find the largest scarp height. The *maximum* heights are based on repeat measurement which are predominantly within ~10 m of each other. This method was chosen because it was not feasible nor within the scope of the study to make cross-sectional profiles along the entire length of each shortening structure to identify the maximum height. Note that the measured heights are not the 'original formation' heights of the scarps, as variable amounts of erosion have occurred across the study area and have thus lowered the heights. This might include erosion between episodes of fault activity on the same structure. Alternatively, there may have been a net deposition of sediment on the down-dropped side, which would also lessen the height difference.

5.2. Comparison to previous structural surveys

Global tectonic trends and orientations on Mars have previously been identified in lower-resolution global surveys (Anderson et al., 2001; Knapmeyer et al., 2006; Tanaka et al., 2014; Watters, 1993) drawing on the 100–300 m/pixel image data sets. In the western hemisphere, thrust-fault related landforms are generally oriented circumferentially to the Tharsis volcano-tectonic province (e.g. Watters, 1993) or are randomly oriented and attributed to global contractional strain (Golombek & Phillips, 2010). The dominant N/S strike of shortening structures in our study area coincides with Tharsis-circumferential orientations.

Shortening structures occur across the study area but are distributed unequally (Supplementary Materials). There appears to be a higher number of structures in the highlands than in the lowlands, with the north and northwest being most sparse. Part of the reason for this is that structures are not clearly discernible in much of the lowlands on visible data products. However, topographic signatures of possible tectonic rises (previously identified by Knapmeyer et al., 2008; Tanaka et al., 2014) are observable underlying a younger textured/fractured mantling deposit in Acidalia Planitia. In contrast to Figure 3, global surveys show a higher number of structures in the Chryse lowlands than the Arabia highlands (Knapmeyer et al., 2006; Tanaka et al., 2014; Tanaka et al., 2005); but this is because they include the mantled tectonic structures in Acidalia Planitia and because the tectonic structures in the highlands are challenging to identify using lower resolution images.

5.3. Applications of this study

Studying tectonic features provides insights into the properties and evolution of Mars' lithosphere and its thermal evolution, contributing to our wider understanding of Mars' geological history. Structural maps are invaluable in deducing the tectonic evolution of a region and provide insights into the timings of tectonic activity and sources of stress. The Map of Tectonic Shortening Structures in Chryse Planitia and Arabia Terra, Mars (Supplementary Materials; Woodley et al., 2023) can be used for global, regional, and local scale studies.

For example, the map suggest that tectonic structures in this region are far more common and widespread than previously reported (Anderson et al., 2008; Knapmeyer et al., 2006; Tanaka et al., 2014; Watters, 1993). If tectonic structures are significantly more common globally, then this has implications for various fields of study including the temporal and spatial distribution of seismicity (Knapmeyer et al., 2006), the magnitude of global contraction (Nahm & Schultz, 2011), and for thermal and geodynamic models (e.g. Hauck & Phillips, 2002). The map can also be used to consider the regional contribution of tectonism to topography, and its implications for estimates of palaeoshoreline displacement (Citron et al., 2018). The data recorded in the shapefile attribute table (Woodley et al., 2023) provides a large morphometric dataset of martian shortening structures and could be used to better understand their formation and subsurface structure. If the timing of tectonic activity can be constrained, then tectonic structures become useful stratigraphic markers that can be used to establish the relative ages of crosscutting/crosscut landforms in the area. In future publications, the above applications of the map will be further explored.

6. Conclusions

A structural map of tectonic shortening structures in Chryse Planitia and Arabia Terra, Mars is presented both as a digital map file map and as a GIS-ready dataset (Supplementary Materials; Woodley et al., 2023). It can be used to aid the understanding of tectonic and

geological process along the dichotomy in Chryse Planitia and Arabia Terra. Based on our interpretive structural-based classification and mapping using high resolution data (up to 6 m/pixel), we conclude that:

- There are 845 identified thrust-fault related landforms, termed shortening structures, in the study area. We find evidence of extensional tectonic structures, but these are too small to be displayed at map publication scale.
- Shortening structures occur across the map area, with a higher structure density in the Arabia Terra highlands than in the Chryse Planitia lowlands.
- Shortening structures have dominant north striking (east dipping) and south striking (west dipping) orientations, broadly in line with circum-Tharsis trends (e.g. Tanaka et al., 2014; Watters, 1993).
- The structural map shows that tectonic landforms are significantly more common in this region than previously reported (Anderson et al., 2008; Knapmeyer et al., 2006; Tanaka et al., 2014; Watters, 1993).

Software

ArcGIS Pro® 2.7.2 software was used to digitise the data and Adobe InDesign® was used to produce the final map sheet.

Acknowledgements

We thank all the scientists and engineers who built CTX and have operated it for over a decade at Malin Space Science Systems and the Jet Propulsion Laboratory, and the Murray Lab for compiling the CTX mosaic dataset.

Disclosure statement

No potential conflict of interest was reported by the author(s).

Funding

We gratefully acknowledge funding from STFC grant ST/V50693X/1 and The Open University STEM Faculty (SZW), UK Space Agency ST/W002736/1 (PF), and ST/R001413/1 (MRB).

Data availability statement

All the data used in this map is freely available. Shortening structure polyline data is available as a shape file (.shp) and associated layer (.lyr) file containing the symbology information from The Open University research repository ORDO (https://ordo.open.ac.uk) using the search term '*Dataset: Structural Map of Tectonic Shortening Structures in Chryse Planitia and Arabia Terra, Mars*' or DOI:10.21954/ou.rd.23143217.

CTX data is available from the Murray Lab (https://murray-lab.caltech.edu/CTX/) or Mars Image Explorer (http://viewer.mars.asu.edu/viewer/ctx#T = 0). HRSC data can be downloaded from the Freie Universitat Berlin (https://maps.planet.fu-berlin.de/#map = 3/2074498.35/0). Data is available from the USGS Astrogeology Science Center for THEMIS (https://astrogeology.usgs.gov/search/map/Mars/Odyssey/THEMIS-IR-Mosaic-ASU/Mars_MO_THEMIS-IR-Day_mosaic_global_100m_v12) and MOLA gridded data (https://astrogeology.usgs.gov/search/map/Mars/GlobalSurveyor/MOLA/Mars_MGS_MOLA_ClrShade_merge_global_463m).

ORCID

Savana Z. Woodley http://orcid.org/0000-0002-4184-6956
Peter Fawdon http://orcid.org/0000-0003-1900-8347
Matthew R. Balme http://orcid.org/0000-0001-5871-7475
David A. Rothery http://orcid.org/0000-0002-9077-3167

References

Anderson, R. C., Dohm, J. M., Golombek, M. P., Haldemann, A. F. C., Franklin, B. J., Tanaka, K. L., Lias, J., & Peer, B. (2001). Primary centers and secondary concentrations of tectonic activity through time in the western hemisphere of Mars. *Journal of Geophysical Research: Planets*, *106*(E9), 20563–20585. https://doi.org/10.1029/2000JE001278

Anderson, R. C., Dohm, J. M., Haldemann, A. F. C., Pounders, E., Golombek, M. P., & Castano, A. (2008). Centers of tectonic activity in the eastern hemisphere of Mars. *Icarus*, *195*(2), 537–546. https://doi.org/10.1016/j.icarus.2007.12.027

Apuzzo, A., Schmidt, G. W., Cianfarra, P., Frigeri, A., Salvini, F., & Scienze, D. (2021). Tectonic-related fractures in Oxia Planum (Mars) and their implication for life investigation. in *52nd Lunar and Planetary Science Conference*. Houston (Virtual), 15–18 March., 2082.

Byrne, P. K., Klimczak, C., Şengör, A. M. C., Solomon, S. C., Watters, T. R., & Hauck, S. A. (2014). Mercury's global contraction much greater than earlier estimates. *Nature Geoscience*, *7*(4), 301–307. https://doi.org/10.1038/ngeo2097

Byrne, P. K., Klimczak, C., & Şengör, A. M. C. (2018). The tectonic character of mercury. In *Mercury: The view after messenger* (pp. 249–286). Cambridge University Press. https://doi.org/10.1017/9781316650684.011.

Christensen, P. R., Jakosky, B. M., Kieffer, H. H., Malin, M. C., McSween, H. Y., Nealson, K., Mehall, G. L., Silverman, S. H., Ferry, S., Caplinger, M., & Ravine, M. (2004). The Thermal Emission Imaging System (THEMIS) for the Mars 2001 Odyssey mission. *Space Science Reviews*, *110* (1/2), 85–130. https://doi.org/10.1023/B:SPAC.0000021008.16305.94

Citron, R. I., Manga, M., & Hemingway, D. J. (2018). Timing of oceans on Mars from shoreline deformation. *Nature*, *555*(7698), 643–646. https://doi.org/10.1038/nature26144

Davis, J. M., Balme, M., Grindrod, P. M., Williams, R. M. E., & Gupta, S. (2016). Extensive Noachian fluvial systems in Arabia Terra: Implications for early Martian climate. *Geology*, *44*(10)), https://doi.org/10.1130/G38247.1

Davis, J. M., Balme, M. R., Fawdon, P., Grindrod, P. M., Favaro, E. A., Banham, S. G., & Thomas, N. (2023). Ancient alluvial plains at Oxia Planum, Mars. *Earth and Planetary Science Letters*, *601*, 117904. https://doi.org/10.1016/j.epsl.2022.117904

Dickson, J. L., Ehlmann, B. L., Kerber, L. H., & Fassett, C. I. (2023). Release of the global CTX mosaic of Mars: An Experiment in information-preserving image data processing. in *54th Lunar and Planetary Science Conference*, 2353. https://doi.org/10.1029/2006JE002808.

Edwards, C. S., Nowicki, K. J., Christensen, P. R., Hill, J., Gorelick, N., & Murray, K. (2011). Mosaicking of global planetary image datasets: 1. Techniques and data processing for Thermal Emission Imaging System (THEMIS) multi-spectral data. *Journal of Geophysical Research*, *116* (E10008), 1–21. https://doi.org/10.1029/2010JE003755

Fawdon, P., Balme, M., Davis, J., Bridges, J., Gupta, S., & Quantin-Nataf, C. (2022). Rivers and lakes in western Arabia Terra: The fluvial catchment of the ExoMars 2022 Rover landing site. *Journal of Geophysical Research: Planets*, *127*(2), e2021JE007045. https://doi.org/10.1029/2021JE007045

Fossen, H. (2010). *Structural Geology*. 1st ed. Cambridge University Press.

Golombek, M., & Phillips, R. (2010). Mars Tectonics. In *Planetary tectonics* (pp. 183–232). 1st ed. Cambridge University Press. https://doi.org/10.1017/CBO9780511691645.

Hartmann, W. K., & Neukum, G. (2001). Cratering chronology and the evolution of Mars. *Space Science Reviews*, *96*(1/4), 165–194. https://doi.org/10.1023/A:1011945222010

Hauck, S. A., & Phillips, R. J. (2002). Thermal and crustal evolution of Mars. *Journal of Geophysical Research*, *107* (E7), 6–1. https://doi.org/10.1029/2001JE001801

Hotine, M. (1946). The orthomorphic projection of the spheroid. *Empire Survey Review*, *8*(62), 300–311. https://doi.org/10.1179/sre.1946.8.62.300

Howard, K., & Muehlberger, W. (1973). Lunar thrust faults in the Taurus-Littrow region. [detected by Apollo 17], *Apollo 17 Preliminary Science Report, NASA Special Publication*. https://ntrs.nasa.gov/citations/19740010359.

Jaumann, R., Neukum, G., Behnke, T., Duxbury, T. C., Eichentopf, K., Flohrer, J., Gasselt, S. V, Giese, B., Gwinner, K., Hauber, E., Hoffmann, H., Hoffmeister, A., Köhler, U., Matz, K.-D., Mccord, T. B., Mertens, V., Oberst, J., Pischel, R., Reiss, D., … Wählisch, M. W. (2007). The high-resolution stereo camera (HRSC) experiment on Mars Express: Instrument aspects and experiment conduct from interplanetary cruise through the nominal mission. *Planetary and Space Science*, *55*(7–8), 928–952. https://doi.org/10.1016/j.pss.2006.12.003

Kim, Y. S., & Sanderson, D. J. (2005). The relationship between displacement and length of faults: A review. *Earth-Science Reviews*, *68*(3–4), 317–334. https://doi.org/10.1016/j.earscirev.2004.06.003

Klimczak, C., Byrne, P. K., Sengör, C. A. M., & Solomon, S. C. (2019). Principles of structural geology on rocky planets. *Canadian Journal of Earth Sciences*, *56*(12), 1437–1457. https://doi.org/10.1139/cjes-2019-0065

Knapmeyer, M., Oberst, J., Hauber, E., Wählisch, M., Deuchler, C., & Wagner, R. (2006). Working models for spatial distribution and level of Mars' seismicity. *Journal of Geophysical Research: Planets*, *111*(E11006). https://doi.org/10.1029/2006JE002708

Knapmeyer, M., Schneider, S., Misun, M., Wählisch, M., & Hauber, E. (2008). An extended global inventory of Mars surface faults. *Geophysical Research Abstracts*, *10*, 11006. https://doi.org/10.1029/2006JE002708

Loveless, S. R., McCullough, L. R., Klimczak, C., Crane, K. T., & Byrne, P. K. (2023). Geomorphology of shortening structures on mercury depicts no grouping into categories. in *54th Lunar and Planetary Science Conference*, 1695.

Lucchitta, B. K. (1976). Mare ridges and related highland scarps - result of vertical tectonism?, In *7th Lunar and Planetary Science Conference*. Houston, 15–18 March., 2761–2782.

Malin, M. C., Bell, J. F., Cantor, B. A., Caplinger, M. A., Calvin, W. M., Clancy, R. T., Edgett, K. S., Edwards, L., Haberle, R. M., James, P. B., Lee, S. W., Ravine, M. A., Thomas, P. C., & Wolff, M. J. (2007). Context Camera investigation on board the Mars Reconnaissance Orbiter. *Journal of Geophysical Research*, *112*(5), 5–9. https://doi.org/10.1029/2006JE002808

Man, B., Rothery, D. A., Balme, M. R., Conway, S. J., Wright, J. (in press). Widespread small grabens consistent with recent tectonism on Mercury. Nature Geoscience.

Nahm, A. L., & Schultz, R. A. (2011). Magnitude of global contraction on Mars from analysis of surface faults: Implications for martian thermal history. *Icarus*, *211* (1), 389–400. https://doi.org/10.1016/j.icarus.2010.11.003

Neukum, G., Jaumann, R., Albertz, J., Bellucci, G., Bibring, J. P., Buchroithner, M., Dorrer, E., Ebner, H., Hauber, E., & Heipke, C. (2004). HRSC: The High Resolution Stereo Camera of Mars Express. In *Mars Express: The Scientific Payload*, Vol 1240.

Quantin-Nataf, C., Carter, J., Mandon, L., Thollot, P., Balme, M., Volat, M., Pan, L., Loizeau, D., Millot, C., Breton, S., Dehouck, E., Fawdon, P., Gupta, S., Davis, J., Grindrod, P. M., Pacifici, A., Bultel, B., Allemand, P., Ody, A., … Broyer, J. (2021). Oxia Planum: The landing site for the ExoMars "Rosalind Franklin" Rover mission: Geological context and prelanding interpretation. *Astrobiology*, *21*(3), 345–366. https://doi.org/10.1089/ast.2019.2191

Schultz, R. A. (2000). Localization of bedding plane slip and backthrust faults above blind thrust faults: Keys to wrinkle ridge structure. *Journal of Geophysical Research: Planets*, *105*(E5), 12035–12052. https://doi.org/10.1029/1999JE001212

Smith, D. E., Zuber, M. T., Frey, H. V., Garvin, J. B., Head, J. W., Muhleman, D. O., Pettengill, G. H., Phillips, R. J., Solomon, S. C., Zwally, H. J., Banerdt, W. B., Duxbury, T. C., Golombek, M. P., Lemoine, F. G., Neumann, G. A., Rowlands, D. D., Aharonson, O., Ford, P. G., Ivanov, A. B., … Sun, X. (2001). Mars Orbiter Laser Altimeter: Experiment summary after the first year of global mapping of Mars. *Journal of Geophysical Research: Planets*, *106*(E10), 23689–23722. https://doi.org/10.1029/2000JE001364

Tanaka, K. L., Skinner, J. A., Dohm, J. M., Irwin, R. P., Kolb, E. J., Fortezzo, C. M., Platz, T., Michael, G. G., & Hare, T. M. (2014). Geologic Map of Mars. *USGS Scientific Investigations Map 3292*.

Tanaka, K. L., Skinner, J. A., & Hare, T. M. (2005). Geologic Map of the northern plains of Mars. *U.S. Geological Survey Geologic Investigations*, SIM 2888, 80225.

Vago, J., Witasse, O., Svedhem, H., Baglioni, P., Haldemann, A., Gianfiglio, G., Blancquaert, T., McCoy, D., & de Groot, R. (2015). ESA ExoMars program: The next step in exploring Mars. *Solar System Research*, *49*(7), 518–528. https://doi.org/10.1134/S0038094615070199

Watters, T. R. (1988). Wrinkle ridge assemblages on the terrestrial planets. *Journal of Geophysical Research: Solid Earth*, *93*(B9), 236–246. https://doi.org/10.1029/JB093iB09p10236

Watters, T. R. (1993). Compressional tectonism on Mars. *Journal of Geophysical Research*, *98*(E9), 17049–17060. https://doi.org/10.1029/93JE01138

Watters, T. R., & Nimmo, F. (2010). The tectonics of Mercury. In T. R. Watters & A. Schultz (Eds.), *Planetary Tectonics* (1st ed., pp. 15–80). Cambridge University Press.

Wellman, J. B., Landauer, F. P., Norris, D. D., & Thorpe, T. E. (1976). The Viking Orbiter Visual Imaging Subsystem. *Journal of Spacecraft and Rockets*, *13*(11), 660–666. https://doi.org/10.2514/3.57128

Woodley, S. Z., Fawdon, P., Balme, M. R., & Rothery, D. A. (2023). Dataset: Tectonic shortening structures in Chryse Planitia and Arabia Terra, Mars. *The Open University*. https://doi.org/10.21954/ou.rd.23143217.